



HAL
open science

Geometric vascular singularities, hemodynamic markers and pathologies

Valerie Deplano, Carine Guivier-Curien

► **To cite this version:**

Valerie Deplano, Carine Guivier-Curien. Geometric vascular singularities, hemodynamic markers and pathologies. Valerie Deplano, Jose-Maria Fullana, Claude Verdier. Biological flow in large vessels; Dialog between numerical modeling and in vitro/in vivo experiment (250pages). Edition ISTE-WILEY. <https://www.iste.co.uk/book.php?id=1883>, Wiley-ISTE; 1er édition (1 juin 2022), 2022, 1789450659. hal-03859548

HAL Id: hal-03859548

<https://hal.science/hal-03859548>

Submitted on 11 Oct 2023

HAL is a multi-disciplinary open access archive for the deposit and dissemination of scientific research documents, whether they are published or not. The documents may come from teaching and research institutions in France or abroad, or from public or private research centers.

L'archive ouverte pluridisciplinaire **HAL**, est destinée au dépôt et à la diffusion de documents scientifiques de niveau recherche, publiés ou non, émanant des établissements d'enseignement et de recherche français ou étrangers, des laboratoires publics ou privés.

3

Vascular Geometric Singularities, Hemodynamic Markers and Pathologies

Valérie DEPLANO and Carine GUIVIER-CURIEN

*CNRS, IRPHE, Ecole Centrale Marseille,
Aix-Marseille University, France*

3.1. Introduction

Vascular pathologies are numerous and varied, and their genesis and development are multifactorial. Nevertheless, it is now known that the characterization and analysis of the fluid dynamics and structures involved in the functioning of certain segments of the vascular system allow their dysfunction to be better understood, and allow correlations to be established between these dynamics and the genesis and development of vascular pathologies.

The purpose of this chapter is to describe flow behaviors in certain geometric singularities of the cardiovascular system, whether they are native or pathological, and to correlate their dynamics with the evolution of cardiovascular pathologies. These correlations can be made using associations between the spatiotemporal distributions of certain hemodynamic markers/indexes and in vivo observation of deleterious clinical events. Certain in silico and in vitro works conducted within the IRPHE Biomechanics team, mostly over the period of the “Biomechanics of fluids and transfers, biological structure-fluid interaction” and “MEChAnics

Biological Flow in Large Vessels,
coordinated by Valérie DEPLANO, José-Maria FULLANA, Claude VERDIER. © ISTE Ltd 2022.

of BIOlogical materials and fluids” research groups, will notably serve to illustrate the remarks, which will not necessarily be exhaustive.

3.2. General characteristics of blood flows at the macroscopic scale

Biomechanical models of blood flows in the cardiovascular system at the macroscopic scale form part of a complex geometric, hydrodynamic and mechanical environment. As the heart delivers a pulsatile flow, blood flows are inherently unsteady. These flows occur in three-dimensional, evolving geometries, a specific patient with many singularities. The behavior of blood, which is closely linked to that of red blood cells, may exhibit a Newtonian, shear-thinning, viscoelastic or even thixotropic nature, depending on the vascular segment. Arterial walls, which are heterogeneous living media, have a visco-hyperelastic anisotropic mechanical behavior. The pulsatile character of flow and the viscoelastic nature of the walls lead to the propagation of pressure and velocity waves along the arterial system. In addition, the presence of geometric singularities induces wave reflections and thus contributes to altering the shape of the waves (pressure and velocity) along the cardiovascular system. It should be noted that these alterations are also due to the dispersive nature of the wall and the nonlinear effects of the pressure/diameter relationship of the artery and the fluid. At the same time, given their spatial proximity, these geometric singularities also result in it being impossible to obtain fully developed flows.

If we consider circulation models with distributed parameters (as opposed to global parameters), the location of the vascular segment to be modeled within the cardiovascular system will therefore play a significant role. As the acceleration and deceleration ramps and the maximum and minimum values of the pressure and velocity waves vary from one site to another in the cardiovascular system, the spatiotemporal shapes of the velocity profiles associated with different areas of the arterial tree cannot be considered to be identical. Furthermore, any dysfunction will also result in an alteration of these spatiotemporal shapes.

In macro-circulation two dimensionless numbers, the Reynolds number, Re , and the frequency parameter, α , or Womersley number, $\vartheta = \alpha^2$, allow the classification of blood flow regimes.

During systolic acceleration, the maximum value of the Reynolds number¹, $Re = \frac{Ud}{\nu}$, can reach 5,000 at the outlet of the left ventricle and flow can remain laminar. By contrast, at the beginning of deceleration, certain authors (McDonald 1952, for example) agree that for a critical Reynolds number value and particular values of the frequency parameter, disturbances appear, leading to a transition to turbulence.

The frequency parameter, which characterizes flow unsteadiness, is defined as $\alpha = a \sqrt{\frac{\omega}{\nu}}$, where a is the radius of the artery and $\omega = \frac{2\pi}{T}$ represents the pulsation. T is generally considered to be the cardiac cycle period. In practice, however, the definition of laws for the transition to turbulence, as well as analysis of evolution mechanisms for secondary structures that exist in certain geometric singularities of the cardiovascular system, in fact involves characteristic times that are related to systolic acceleration or deceleration times. It should be noted, for example, that the appearance of turbulence during the deceleration phase and the ensuing relaminarization are strongly dependent on the deceleration ramps. A longer deceleration time allows instabilities created at the wall to propagate toward the tube axis, whereas a shorter time results in a faster relaminarization.

The Womersley number can also be written as the ratio of characteristic times. Thus, $\vartheta = \alpha^2 = \frac{a^2/\nu}{1/\omega}$ represents the viscous diffusion time over the period of motion. If, as a first approach, we consider that blood viscosity and the cardiac period remain constant throughout the cardiovascular system, then only the radius of the artery of the site concerned influences this parameter. Therefore, for arteries with large diameters, of the order of 1 cm, the frequency parameter will be higher than for arteries with smaller dimensions and the viscous diffusion time will be large relative to the period of motion. The boundary layer will be confined to the wall and the velocity profiles will have a somewhat plateau shape, regardless of the effects of inlet, setting in motion or the appearance of a turbulent regime. In coronaries, which are arteries with smaller diameters, ~ 3 mm, the frequency parameter value will be lower, the viscous diffusion time will be low compared to the period of motion, the boundary layer will develop faster and thus the velocity profiles will have a more parabolic shape.

¹ ρ density of blood, ν its kinematic viscosity, U its average velocity, and d the artery diameter.

This analysis is supported by a dimensional study of the thickness of the Stokes layer, $\delta_s = \left(\frac{\nu}{\omega}\right)^{1/2} = \frac{a}{\alpha}$. The thickness of the boundary layer is all the thinner (or more developed, respectively), the larger the frequency parameter is (or smaller, respectively).

Table 3.1 gives several mean values of Re and α encountered in different segments of the arterial tree, considering a constant dynamic viscosity value equal to 3.6×10^{-3} Pa·s, the density of blood, $\rho = 1,060$ kg/m³, and the cardiac period, $T = 0.8$ s.

	Diameter	Re_{ave}	α
Ascending thoracic aorta	~25 mm	1472.2	19
Abdominal aorta	~18 mm	1,060	13.6
Right coronary artery (RCA)	~3.7 mm	261.4	2.8

Table 3.1. Several characteristic values of the Reynolds number and frequency parameter in macrocirculation

The Dean and Strouhal numbers are also used in the characterization of secondary vortical structures (VSS) that appear downstream of geometric singularities, whether native or pathological. Dean (1928) was one of the first to describe the counter-rotating helical structures existing in the aortic arch. The Dean number, defined as $De = Re \sqrt{H}$, allows consideration of the aspect ratio, H , between the radius of the artery, a , and its radius of curvature, R , $H = \frac{a}{R}$. It measures the ratio of the centrifugal inertial forces to the viscous forces. Within the context of biofluid mechanics, the Strouhal number, $S_t = \frac{f D_r}{U}$, is also used to quantify the frequency, f , of the detachment of vortex rings downstream of the orifice, where D_r is the constriction diameter and U the upstream flow velocity.

The general characteristics of blood flows have been presented succinctly. Nevertheless, these elements make it easier to address one of the main objectives of this chapter, focusing on the analysis of the relationships existing between the dynamics of blood flows in certain geometric singularities, the determination of hemodynamic markers associated with the behavior of these dynamics and the evolution of vascular pathologies. The

physical phenomena and subsequent behaviors of blood flows in the most common macroscopic singularities of the cardiovascular system are presented in the following section. The purpose is not to provide an exhaustive review but to describe the main physical phenomena.

3.3. Several geometric singularities of the cardiovascular system

The physiological singularities that will induce particularities in flow behavior are mainly those correlated with the existence of curvatures and bifurcations, that is, a change in flow direction. The valves also induce hemodynamic specificities linked to a significant dynamic variation in the diameter of the arterial lumen, from approximately 21–22 mm (Oh *et al.* 1999) in systole to 0 mm in diastole through the valve leaflets. The most notable pathological particularities are correlated with cross-section enlargements and constrictions, which are found in many pathologies. The most evident are aneurysms and valve or artery stenoses, regardless of their locations. Other conditions, such as aortic dissection and aortic coarctation, also induce cross-section enlargements and constrictions. These particularities can be combined: notably, cross-section constriction followed by an enlargement or a curvature. We must note that vessel tortuosities, which may be physiological or pathological, are, quite simply, curvatures. Finally, prosthetic particularities also induce alterations in blood flow behavior. Examples include bypass surgery, stents, endoprotheses, mechanical or bioprosthesis valves. Only valve prostheses will be described in this chapter.

3.3.1. Curvatures and bifurcations

The characteristics of the aortic arch mean it is considered to be a duct of great curvature with an average curvature ratio, H , between $\frac{1}{4}$ and $\frac{1}{2}$. In addition, there are many bifurcations in the vascular system, with these feeding adjacent organs. Starting from the aorta, for example: the brachiocephalic arterial trunk, the left primitive carotid and the left and right subclavians irrigate the head, neck and upper limbs, the renal arteries that bifurcate from the abdominal aorta vascularize the kidneys, the iliac bifurcation feeds the lower limbs, etc.

Generically speaking, curved or bifurcated geometries induce a change in fluid direction, initially straight, giving rise to a centrifugal force directed

from the inner wall of the curved duct (or outer of the daughter branch of the bifurcation) to the outer wall. In addition to the viscosity forces, the fluid motion is then governed by the relationship between the centrifugal forces and the transverse pressure gradient, which is in the opposite direction. Flows in bent or bifurcated geometries were extensively studied by Pedley (1980).

To describe the characteristics of this flow type in the center plane of symmetry (r, θ) (Figure 3.1(a)) as simply as possible, let us assume that at inlet there is a plateau-type velocity profile with a thin wall boundary layer corresponding to a high frequency-parameter value. Such a scenario is quite likely in the aortic arch as in the parent branch of the iliac bifurcation, that is, the abdominal aorta. In this case, for most of the tube the flow can be considered as inviscid; the pressure increases upon moving away from the center of curvature and by applying Bernoulli, in the center plane, the maximum axial velocity is initially located toward the inner wall of the curved duct. Then downstream, with the development of the boundary layer toward the center of the curved duct, this maximum velocity is offset toward the outer wall; in the boundary layer the centrifugal force induces a motion of fluid directed toward the outer wall. Boundary layers play an important role in the development of three-dimensional effects.

In the center plane, where the axial velocity amplitudes are highest, the centrifugal forces are predominant on the pressure gradient leading to a motion directed toward the outer wall of the tube. In the lower and upper planes, the decrease in velocity amplitude is accompanied by the domination of the transverse pressure gradient and the fluid motions directed toward the interior wall (Figure 3.1(b)). The composition of these opposing motions gives rise to a secondary flow in the form of two counter-rotating vortices, which develop in planes perpendicular to the axial flow and propagate helically.

It seems important to describe some characteristics associated with bifurcations that depend on geometric factors such as the bifurcation angle, β , or the ratio, R_s , between the daughter branch diameter, D_d , and the radius of the parent branch, a_p as well as the flow regime. In general, recirculating regions appear along the outer walls if the ratio, R_s , is greater than 1. The extent of the recirculating regions is accentuated with the increase in the Re number, but also with the bifurcation angle.

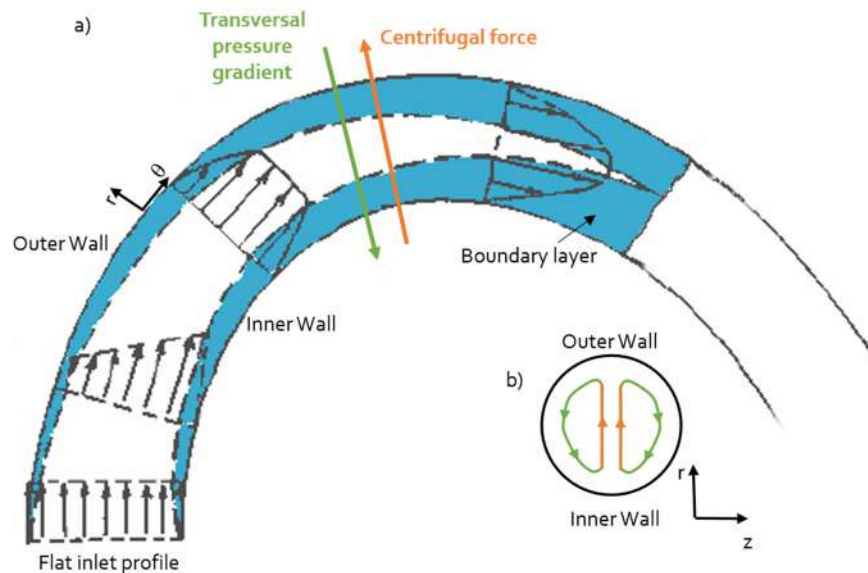


Figure 3.1. Representative diagram of a) main and b) secondary flows in a singularity with change of direction. Steady flow. Adapted from Fung (1996). For a color version of this figure, see www.iste.co.uk/deplano/biological.zip

All of these characteristics evolve during the cardiac cycle. The dynamic evolution of counter-rotating vortices may, for example, be described in different cross-sections, θ , perpendicular to the main flow as a function of the instant considered in the cardiac cycle. It is dependent on the inlet velocity conditions as well as the De and α numbers. Thus, in parallel with the description of these structures with two counter-rotating vortices, works conducted in the 1980s (Masliyah 1980; Dennis and Ng 1982; Cheng and Mok 1986) show that, based on a critical value of the Dean number of the order of 950, a dual solution exists, consisting of four counter-rotating vortices. The existence of secondary flows with two additional vortices, stable or unstable, appears to be due to centrifugal instabilities.

The works, in vitro and in silico, carried out by Boiron *et al.* (2007) in a bent tube by considering physiological flows, make it possible to illustrate the evolution of secondary structures in an idealized aortic arch model.

For small values of the Dean number, $De = 114$, and the frequency parameter, $\alpha = 8.14$ (Figure 3.2), during systolic acceleration, we observe

the development of two circumferential motions along the side walls. These motions, which remain confined in the viscous layer, are directed from the outer wall to the inner wall. Given the low value of α , the viscous diffusion time is low relative to the period of motion, which induces a viscous layer thickness of the order of one-third of the radius at $\theta = 156^\circ$. At maximum flow ($t = 0.528$ s), these motions impact at the inner wall and give rise to two counter-rotating vortices that move from the inner wall to the outer wall. The development of these vortices may be likened to a “mushroom” shape. At the start of systolic deceleration, $t = 0.79$ s, these vortices extend radially to occupy almost the entire cross-section. Their intensities then decrease.

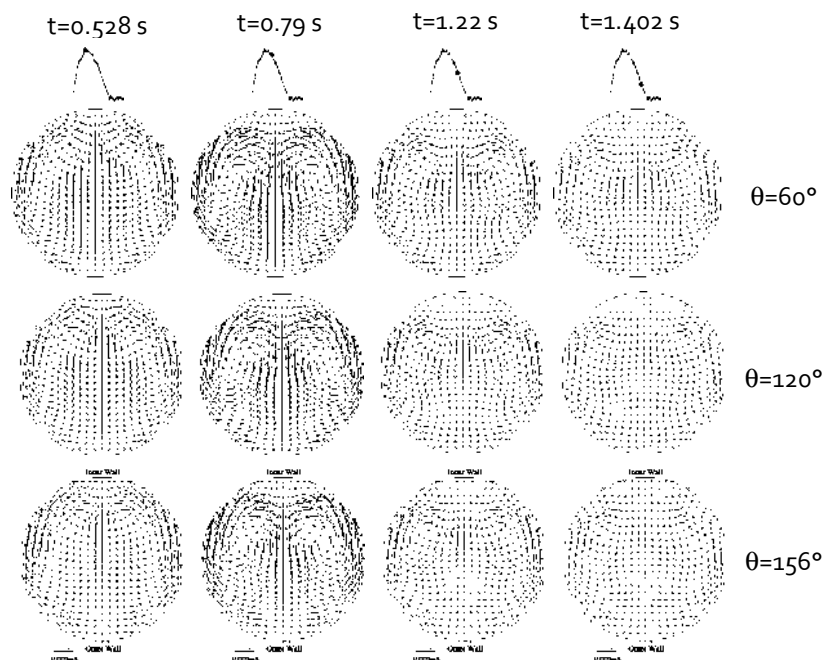


Figure 3.2. Time evolution of velocity vectors in the planes $\theta = 60^\circ$, $\theta = 120^\circ$, $\theta = 156^\circ$, $De = 114$, $\alpha = 8.14$

For the same frequency parameter value, $\alpha = 8.14$, but for a higher value of the Dean number, $De = 210$ (Figure 3.3), the intensity of the counter-rotating vortices is greater but they remain confined to the upper part of the cross-section throughout the acceleration phase, $t < 0.565$ s. When the flow decelerates, 0.79 s $< t < 1.24$ s, the vortices extend toward the outer

wall. For $\theta < 120^\circ$, due to the presence of a radial pressure gradient near the axis of symmetry, they are pushed toward the side walls. These structures, which can be likened to “bean” shapes, belong, according to the Sudo classification (Sudo *et al.* 1992), to structures called deformed Dean circulation. For $\theta = 156^\circ$, two additional counter-rotating vortices, rotating in the opposite direction to the first two, are worth noting. They are associated with structures, which are called intermediate circulation between Dean and Lyne (Lyne 1971).

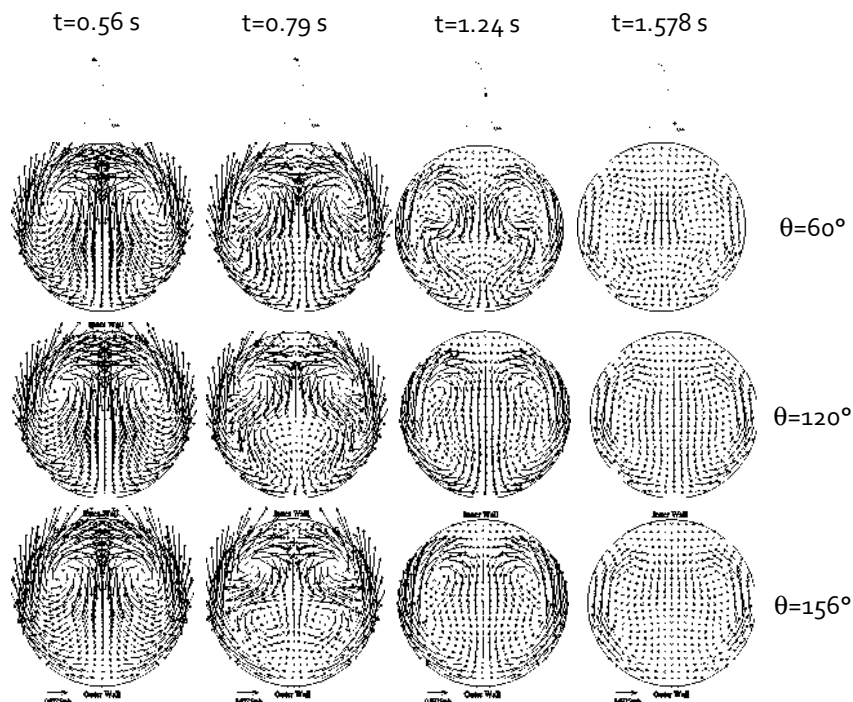


Figure 3.3. Time evolution of the velocity vectors in the planes $\theta = 60^\circ$, $\theta = 120^\circ$, $\theta = 156^\circ$, $De = 210$, $\alpha = 8.14$

These results obtained *in silico* have been confirmed by *in vitro* measurements and visualizations (Boiron *et al.* 2007). The complexity of the spatiotemporal dynamics of these secondary structures according to hydrodynamic conditions offers an indication of the importance for patients of biomechanical models that closely resemble reality.

3.3.2. Cross-section constriction

The flow in a cross-section constriction, representative of arterial stenosis, for example, is equivalent to the flow in a convergent followed by a divergent. Its description in the center plane (Figure 3.4) is facilitated with the use of the rotational transport equation, $\Omega(X, t)$.

$$\frac{\partial}{\partial t}(\Omega) + (V \cdot \nabla)\Omega = (\Omega \cdot \nabla)V + \nu \Delta(\Omega)$$

Upstream of the convergent, flow is irrotational. When the fluid arrives in the convergent, it undergoes continuous acceleration and subsequently, rotational convection takes place toward the low-velocity zones. The convection terms of the rotational equation are opposed to the diffusion terms and reduce the viscous layer to an increasingly small thickness along the convergent. This phenomenon is accentuated by the extension term of the vortex lines, which is directed toward the wall. The velocity profiles then show a central plateau whose width increases upon moving toward the convergent throat. At the throat, the area of the minimum cross-section, the flow has the characteristics of a wall boundary layer, which will be thinner, the higher the Reynolds number.

In the convergent, we can observe a cone of potential fluid whose base lies in the vicinity of the throat.

In the divergent, the convection of the rotational, which takes place toward the center of the tube, will add to its diffusion from the wall and to the extension of the vortex lines, which is directed toward the axis. In the case of the free jet, there is therefore a rotational supplement, which penetrates the potential core and reduces its length. In combination with the decrease in mean velocity, the fluid is subjected to an increase in pressure, which induces a detachment of the boundary layer and the creation of recirculating regions at near-wall negative velocities. The position of the reattachment point, downstream of the neck, is a function of the Reynolds number.

The boundary layer is transformed into a free shear layer that separates the potential core from the region with negative velocities near the walls. It is limited downstream of the neck by the reattachment point, which is not

fixed and oscillates constantly over time. The shear layer transforms into a boundary layer again by reattachment to the wall.

Three main regions can thus be differentiated by moving upstream and downstream: the recirculating region, the reattachment area and the recovery area. It is important to note the sensitivity of post-stenotic flows, via the shear layer, to very small disturbances that can generate convective-type instabilities that “self-maintain” through the recirculating regions, as well as the amplifying nature of instabilities of stenosis.

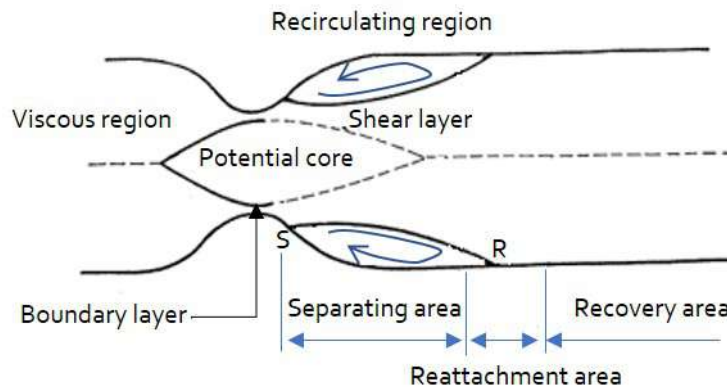


Figure 3.4. Diagram of the main flows in the center plane of a stenosis. S, detachment point of the boundary layer; R, reattachment point. Adapted from Siouffi (1988)

The Re and α values, the spatiotemporal form of the inlet flow rate and the form and degree of severity of stenosis, have an influence on the dynamics of post-stenotic flows. The characterization of the lesion influence lengths and the temporal and spatial evolutions of vortex shedding in the recirculating regions, reattachment points and detachment can be described using the rotational transport equation in a dimensionless form

$$\alpha^2 \frac{\partial}{\partial t} (\Omega^*) + 2Re_{\max} (\mathbf{V} \cdot \nabla) \Omega^* = 2Re_{\max} (\Omega^* \cdot \nabla) \mathbf{V} + \nu \Delta (\Omega^*)$$

The extension term of the vortex lines $(\Omega^* \cdot \nabla) \mathbf{V}$, as well as the term relating to the convection of the rotational $(\mathbf{V} \cdot \nabla) \Omega^*$, increase with the value

of Re_{\max} . Thus, the longitudinal dimension of the recirculating region increases as the maximum Reynolds value increases. The propagation of the recirculating region is then facilitated by an increase in Re_{\max} . If we also consider the rotational transport time, the longitudinal and radial amplitude of the recirculating region will be greater at the beginning of deceleration. The studies of Siouffi *et al.* (1998), carried out by modifying the value of the frequency parameter, however, show that increasing this value leads to a reduction in the recirculating region.

During the flow deceleration phase, the shear layer bordering the potential core will roll up to form a vortex ring downstream of the stenosis neck. The formation and evolution of this ring will be described in section 3.3.3, devoted to cross-section enlargements. The works of Kim *et al.* (2016) enable it to be viewed by MRI, for example. The studies of Zhu *et al.* (2018), meanwhile, demonstrate the complexities of the flows resulting from the serial combination of a stenosis followed by a curvature.

3.3.3. Cross-section enlargement

The flow in a cross-section enlargement is representative of that occurring in fusiform aneurysms, for example. It has characteristics in common with post-stenotic flow, notably with regard to the creation of a jet and the appearance of VSs in the form of a vortex ring downstream of the neck. However, the pre-constriction convergent effects are not present and the effects of the divergent are more pronounced.

As with other singularities, the flow dynamics in cross-section enlargements will depend on the Re number, the frequency parameter, α , but also on the geometric characteristics of the enlargement, such as its dilatation, length, asymmetry and aspect ratio. Nevertheless, a general description can be given.

The cross-section enlargement associated with the flow acceleration phase leads to an irrotational jet flow that enters the divergent. During this phase, the flow remains attached to the wall. At the beginning of deceleration, the velocity discontinuity at the edge of the jet generates an unstable Kelvin–Helmholtz-type shear layer that rolls into a vortex, which detaches at the neck of the divergent and propagates downstream. During the deceleration phase, recirculating regions appear in the zones furthest from the jet axis. The propagation of the ring may, depending on the

hydrodynamic, geometric and rheological conditions, result in an impact of the structure at the wall in the distal region with the appearance of a stagnation point, but also in a near-wall dislocation. It is also important to note that several rings can coexist during a cardiac cycle, depending on the propagation time of the structures.

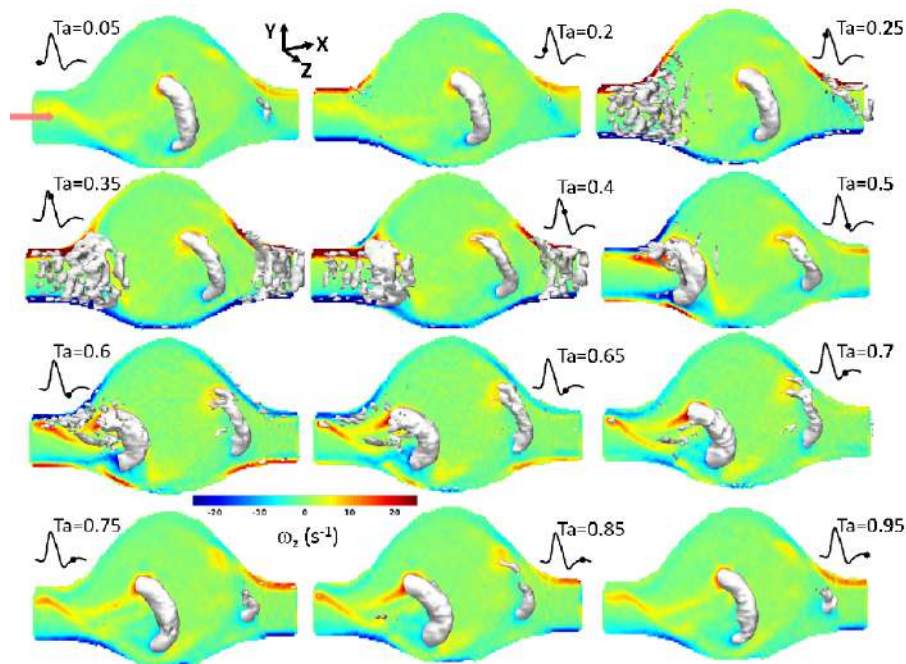


Figure 3.5. 3D temporal evolution of the vortex ring (in gray) overlaid on vorticity maps in the center plane. Adapted from Deplano *et al.* (2016). For a color version of this figure, see www.iste.co.uk/deplano/biological.zip

The *in vitro* works of Deplano *et al.* (2007, 2014, 2016) notably enable the dynamics and propagation of this ring to be quantified by performing velocity measurements using stereo-PIV in a deformable asymmetric aneurysm model for physiological 3D flows and a fluid with shear-thinning behavior. The dynamics of VSs are described and quantified using the criterion λ_{ci} from the works of Zhou *et al.* (1999), which allows structures with local rotation to be extracted from vorticity maps. Figure 3.5 shows the

propagation of vortex rings, identified by 3D isocontours of λ_{ci} overlaid on the vorticity maps in the center plane. These VSs may be involved in the formation of thrombus in the aneurysm sac according to mechanisms, notably associated with the transport of platelet elements (see section 3.5.2.3).

3.3.4. Valves

The aortic valve is the first singularity encountered by the flow in the systemic vascular system. It is located at the aortic root, between the left ventricle and the aorta. This valve is generally composed of three flexible, deformable leaflets (tricuspid valve) but may sometimes have only two leaflets (bicuspid) or even just one (unicuspid) in rare cases (Novaro *et al.* 2003). Behind each of these leaflets, an anatomical bulge, the Valsalva sinus, is present, ending the junction with the aorta. The diameter of the sinotubular junction, downstream of the aortic root, is slightly larger than that of the valve orifice.

The two main characteristics of aortic trans-valvular flows are the formation of a jet through the valve orifice and the presence of vortex structures in the sinuses.

The left ventricular outflow tract ends with the valve orifice, thus creating a constriction. Moreover, the leaflets confine the trans-valvular flow, the streamlines are straight and parallel. Thus, during the systolic phase, a flow in the form of a jet is established through the valve. The opening surface of the valve is quasi-circular, which leads to the formation of a jet centered on the orifice with velocities of the order of 0.8–1.2 m/s. The flow in the ascending aorta is then preferentially aligned with the aortic walls. Generally referred to as symmetric, the jet may nevertheless impact the anterior distal wall of the ascending aorta, according to the latter's curvature in relation to the valve orifice. The downstream cross-section enlargement of the aortic root associated with the curvature of the ascending aorta leads to the development of a secondary helical motion in the ascending aorta from the systolic peak (see section on curvatures and bifurcations) (Kilner *et al.* 1993; Morbiducci *et al.* 2011). This motion is visible during the entire deceleration phase.

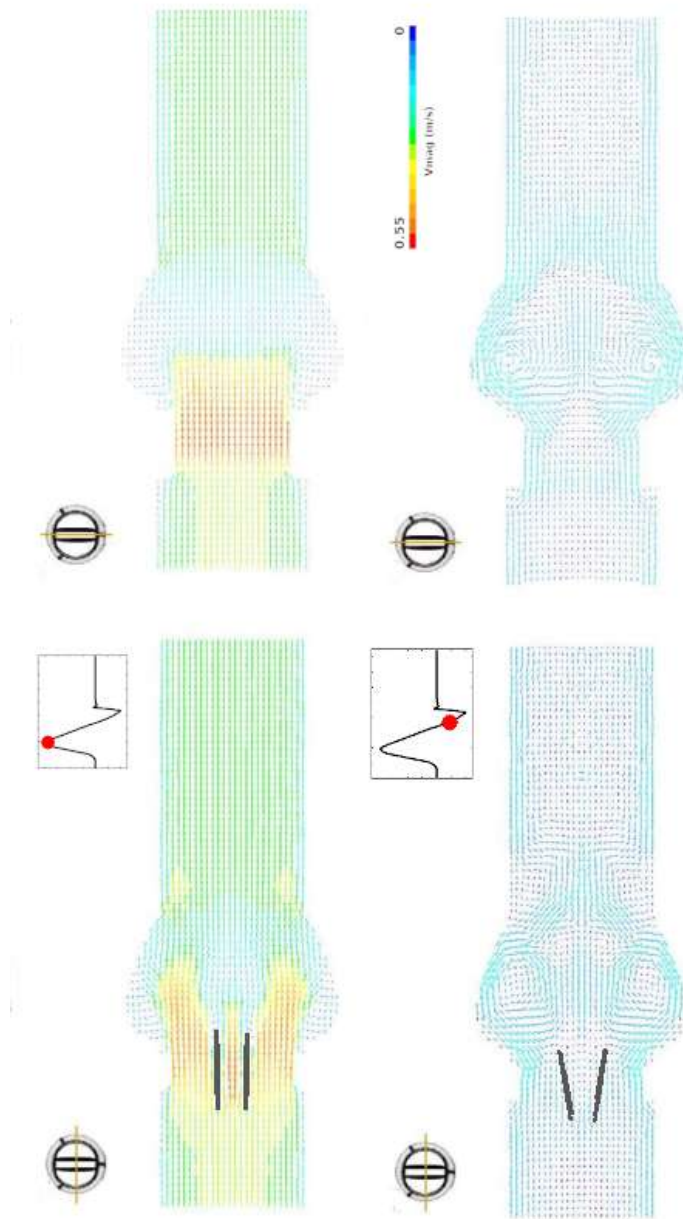


Figure 3.6. Temporal evolution of velocity vectors through a bileaflet prosthetic valve in two perpendicular planes. Adapted from Guivier et al. (2009). For a color version of this figure, see www.iste.co.uk/deplano/biological.zip

In bicuspid cases, two of the three leaflets are fused together, creating an eccentric opening in the aortic root. The dynamics of the transvalvular jet then differ from that observed in the case of a healthy tricuspid valve. The jet is eccentric and asymmetric in the ascending aorta (Hope *et al.* 2011). According to the fused leaflets, the jet directly impacts the anterior wall of the proximal ascending aorta (in the case of a bicuspid with right and left leaflet fusion) or the posterior wall, before being deflected toward the anterior wall (in the case of a bicuspid with right, non-coronary leaflet fusion) (Rodríguez-Palomares *et al.* 2018). Successive deviations and impacts in the curved geometry of the ascending aorta lead to the appearance of a highly helical secondary flow, mainly in patients with a fusion of the right and non-coronary leaflet (Meierhofer *et al.* 2013; Mahadevia *et al.* 2014). Given the geometric angulation of the aorta associated with helical motion, it has been possible to observe retrograde flows in some patients (Barker *et al.* 2010) during the systolic phase.

In case of failure (a problem with closure-regurgitation or with optimal opening – stenosis – calcification, etc.), the aortic valve is replaced with a bioprosthesis or mechanical prosthesis. The design of mechanical valves differs from one prosthesis to another, thus resulting in the behaviors of prosthesis-dependent flows (Dasi *et al.* 2009), whose main characteristics are visible from the systolic peak. In the case of a monoleaflet valve, the orifice is divided into two geometrically asymmetric parts. The result is the formation of two jets of marked, very different amplitudes. The velocity profiles are eccentric in the proximal ascending aorta. In the case of a bileaflet valve, two lateral orifices and one central orifice lead to the formation of three separate jets, also making the flow non-axisymmetric (Figure 3.6). Due to the cross-section constrictions related to the valve design, the recorded velocities are generally higher. At about two diameters downstream of the prosthesis, the velocity profiles become more or less dampened (Yoganathan *et al.* 1986; Hasenkam *et al.* 1988).

During systolic ejection, the free edge of the leaflets of the native or prosthetic aortic valve is not in contact with the wall, given the presence of the sinus behind each of the leaflets. The streamlines are parallel to the leaflets in the valve orifice. Upon reaching the free ends of the leaflets, the streamlines separate to enter the sinuses, resulting in the formation of a recirculating region from the start of the ejection. The vortex structure created is present until the start of diastole. With the closure of the leaflets,

each of the vortex structures gradually extends out of the sinuses, decreasing in intensity. Their presence ensures good cleaning and prevents the post-valvular stasis zones during diastole.

3.4. Hemodynamic markers

Quantified characterizations, *in vitro* or *in silico*, of the flow dynamics in geometric models that are close to vascular pathologies by deploying biomechanical models, taking into account the hydrodynamic conditions of patients, the blood shear-thinning behavior and the wall dilatation capabilities, allow the definition of hemodynamic indexes that are capable of providing relevant response elements in predicting the evolution of these pathologies. Among the most widely-used hemodynamic markers are those derived from the spatiotemporal quantification of wall shear stress and those related to the dynamics of secondary structures. The determination of spatiotemporal mapping of wall shear stress as well as secondary vortical and/or helical structures is notably related to velocity gradients and possible viscosity variations. These two quantities are associated with the geometric singularities that, as we have just shown, significantly influence flow dynamics.

Thus, without quantifying a wall shear stress value, it is important to recall that for curvatures or bifurcations, the location of the maximum velocities, alternately on the inner and/or outer walls, will be associated with regions of high wall shear stress values, and the opposite outer and inner walls, respectively, at lower values; recirculating regions that exist downstream of cross-section constriction (stenosis, coarctation, false lumen of aortic dissection, etc.) but also possibly at the outer walls of bifurcation, as well as within cross-section enlargement (Valsalva sinus, aneurysms, etc.) will lead to low, oscillating wall shear stress values; flow impact zones, such as the apex of a bifurcation or the anterior distal wall of the ascending aorta, will be the site of high wall shear stress values relative to the normal, as will arterial stenosis necks, aortic dissection entry tears or mechanical valve leaflets. VVs, meanwhile, which appear in many singularities, allow for the characterization of complex fluid transport. They will be able to interact with cellular/globular elements – transport them and shear them – and the vascular walls by, for example, impacting them.

3.4.1. Indexes derived from wall shear stress

The indication that we can correlate wall shear stress values with the location of certain vascular pathologies dates back about 50 years. It was mainly dedicated to the analysis of zones prone to the development of atherosclerosis. Although the genesis and development of this pathology depend on many biological factors and involve different spatiotemporal scales, it was noted that there are preferred locations at sites of bifurcations, curvature and constrictions, beyond patient profile – excess lipids in blood (LDL-cholesterol), sedentariness, presence of free radicals due to tobacco, hypertension, diabetes, genetic alteration, stress, etc. As we have seen, these geometric singularities are prone to the appearance of zones of high velocities, recirculation, stases, stagnation points, reattachment points, and helical secondary structures, and these flow particularities induce specificities in wall shear stress behavior.

This indication is currently reflected in the characterization of the spatiotemporal evolution of wall shear stress and its numerous derivative indexes, with associated events involved in a deleterious remodeling of the wall, as we will see in section 3.5.

3.4.1.1. Definitions

Let \mathbf{df} be the elementary shear stress force, τ the viscous stress tensor and \mathbf{n} the external normal to the surface element, ds , on which the elementary wall shear stress force is determined.

$$\mathbf{df} \text{ is defined as } \mathbf{df} = \tau \mathbf{n} ds$$

Considering that fluid has a generalized Newtonian behavior, τ is written as:

$$\tau = 2\mu(J_2)D \text{ with } D \text{ the strain velocity tensor, } D = \frac{1}{2}(\nabla\mathbf{V} + \nabla\mathbf{V}^t) \text{ and } J_2 \text{ its second invariant.}$$

The wall shear stress vector thus defined will be noted \mathbf{WSS} for the remainder of this chapter. It depends on t and the geometric coordinates in which the object of study is defined; $\mathbf{WSS}(\mathbf{X},t)$. It is, therefore, important to quantify its amplitude, direction, spatiotemporal evolution and its variations in relation to its average, its average direction and the associated spatial and temporal gradients.

The markers most commonly used in the literature to associate **WSS** with the location of deleterious clinical events, derived from the **WSS** quantification, are listed below.

The time average of the **WSS** norm, TAWSS (Time Average Wall Shear Stress), is an index introduced by Ku *et al.* (1985). It is defined as:

$$\text{TAWSS} = \overline{\mathbf{WSS}} = \frac{1}{T} \int_0^T |\mathbf{WSS}| dt, \text{ with } |\mathbf{WSS}| \text{ the } \mathbf{WSS} \text{ norm.}$$

The oscillatory shear index (OSI) (Ku *et al.* 1985) represents the degree of deviation of wall shear stress from its mean direction. Its value varies between 0 when the **WSS** is unidirectional and 0.5 when the **WSS** is highly oscillating. This index is written as:

$$\text{OSI} = \frac{1}{2} \left(1 - \frac{\left| \int_0^T \mathbf{WSS} dt \right|}{\int_0^T |\mathbf{WSS}| dt} \right)$$

The **WSS** spatial gradient, WSSG, is a concept introduced by Lei *et al.* (1996). Its components, WSSG_{ij}, are written as:

$$\text{WSSG}_{ij} = \frac{\partial \text{WSS}_i}{\partial x_j}$$

Relative residence time (RRT) is an index proposed by Himburg *et al.* (2004); it is proportional to the residence time of blood particles. It is defined as:

$$\text{RRT} = (1 - 2\text{OSI})\text{TAWSS}$$

Some authors suggest combinations of these indexes. The following can be found, for example:

The Holmes (High Oscillatory Low Magnitude Shear) indicator, introduced by Alimohammadi *et al.* in 2016 (Alimohammadi *et al.* 2016), that identifies zones of low TAWSS and high OSI values. HOLMES = TAWSS(0.5 - OSI)

The degree of deviation of the wall shear stress gradient (WSSG) from its mean direction, gradient oscillatory number (GON), is proposed by

Shimogonya *et al.* (2009):
$$\text{GON} = \frac{1}{2} \left(1 - \frac{\left| \int_0^T \text{WSSG} dt \right|}{\int_0^T |\text{WSSG}| dt} \right)$$

The transWSS is presented by Peiffer *et al.* (2013a), who identifies the temporal variations of the components of the **WSS** perpendicular to the average principal direction.

3.4.2. Indexes describing VSs

The creation and evolution of secondary VSs can also play an important role in the functioning or dysfunction of the cardiovascular system. Their positive role can be found in the left ventricle, with their involvement in a washing function. Their deleterious effects are described in their participation in the formation of thrombotic material, but also in their involvement in various arterial dilatation processes.

The quantification and identification of these coherent structures are derived from works stemming from fluid mechanics (Zhou *et al.* 1999; Chakraborty *et al.* 2005). Vorticity $\boldsymbol{\Omega} = \text{rot}(\mathbf{V})$ alone will not suffice to extract them; indeed, in the near-wall, for example, there are high-vorticity zones due to shearing, associated with viscous dissipation and not with local rotation.

Of the many techniques proposed, none achieve unanimity because they are based on velocity and pressure, which are global quantities. Those calculated from the eigenvalues of the velocity gradient tensor, $\nabla\mathbf{V}$, are used in particular because the complex eigenvalues delimit zones where the streamlines are locally circular or spiral in shape (Chong *et al.* 1990).

$\nabla\mathbf{V}$ can be broken down into a symmetric part, D , the strain velocity tensor, and an antisymmetric part, Ω , the vorticity tensor (or rotation rate): $\nabla\mathbf{V} = D + \Omega$.

The characteristic equation of eigenvalues, λ , of $\nabla\mathbf{V}$ is written as: $\lambda^3 + P\lambda^2 + Q\lambda + R = 0$

For an incompressible flow, $P = -\text{div}\mathbf{V}$, the first invariant $\nabla\mathbf{V}$ is therefore zero. The second and third invariants, Q and R , are defined as:

$$Q = \frac{1}{2} (\|\Omega\|^2 - \|D\|^2) \text{ and } R = -\det(\nabla\mathbf{V})$$

Several criteria deriving from the characteristic equation are used in our scope. The criteria Δ , Q and λ_{ci} are presented below.

The eigenvalues of $\nabla\mathbf{V}$ are complex when Δ , the discriminant of the characteristic equation, is strictly positive. Thus, $\Delta > 0$ constitutes the first criterion for extracting a vortex.

When the second invariant, Q , is strictly positive, the vorticity (antisymmetric part of $\nabla\mathbf{V}$) dominates the strain velocity tensor (symmetric part of $\nabla\mathbf{V}$). Hunt *et al.* (1988) propose that the vortices then be identified by regions that fulfill the strictly positive Q-criterion.

Introduced by Zhou *et al.* (1999), the criterion λ_{ci} (swirling strength) is based on the criterion Δ . The eigenvectors associated with the complex eigenvalues of $\nabla\mathbf{V}$ enable the plane in which the flow is locally swirling to be defined. The criterion λ_{ci} then consists of determining the imaginary part of the complex eigenvalues that represents a local quantification of the vortex motion.

These criteria, based on invariants, have the advantage of being objective quantities and are therefore frame-independent. Moreover, being based solely on the calculation of complex eigenvalues they thus eliminate vorticity regions without local rotation motion, such as shear zones.

Some authors use the criterion λ_2 (Biasetti *et al.* 2011; Ab Naim *et al.* 2016). Based on the fact that the value of the pressure induced locally by the presence of a vortex is minimal, Jeong *et al.* (1995) propose evaluating the eigenvalues of the tensor $D^2 + \Omega^2$. This tensor is derived from the gradient of the Navier–Stokes equation, broken down into symmetric and antisymmetric parts and overlooking the viscous and unsteady effects, which can suppress or generate minimum pressure values, respectively.

Thus, under these hypotheses $D^2 + \Omega^2 = -\frac{1}{\rho}\nabla(\nabla\mathbf{p})$. A local minimum pressure appears if $D^2 + \Omega^2$ has two negative eigenvalues. Since this tensor is symmetric, its eigenvalues are all real. By ordering $\lambda_1 > \lambda_2 > \lambda_3$, the criterion becomes $\lambda_2 < 0$ to have a local minimum pressure due to a vortex only.

Other authors use Lagrangian techniques such as the “Finite-Time Lyapunov Exponent” (FTLE) to extract coherent structures (Shadden and Taylor 2008). The review by Haller (2015) details the latest developments. Arzani and Shadden (2012a), Arzani and Shadden (2012b) and Joly *et al.* (2018)

notably deploy them in the context of the study of aneurysms to describe flow topology.

Finally, based on the quantification of velocity and vorticity fields and their scalar product, criteria such as the normalized helicity index (LNH) or the helicity flow index (HFI) (Grigoni *et al.* 2005; Morbiducci *et al.* 2009) have also been proposed to define the helical motions present in the vascular system.

3.5. Correlation between hemodynamic markers and pathologies: some examples

From the 1970s, different hypotheses were presented to correlate wall shear stress values with atherosclerosis. Fry (1968) claimed that high values could damage endothelial cells and subsequently lead to the stripping of the endothelium, which was thought to be the initiator of the pathology. Conversely, Caro *et al.* (1971) proposed a correlation between low wall shear stress values and pathology development by observation of preferred lesion locations.

Fifty or so years later, the hypothesis of low values of wall shear stress prevails in the mechanisms of atherosclerosis development. This initial hypothesis suggested that low wall shear stress values could lead to prolonged residence times (RRTs) of LDL lipoproteins and/or monocytes and thus promote their local adhesion and infiltration into the arterial wall, characteristic of the pathology (Hermann *et al.* 1994). This increased permeability was seen as responsible for a cascade of deleterious events leading to a remodeling of the wall, such as intimal thickening. This reasoning was also extended to an effect on mass transfers resulting in the local accumulation of growth factors in the proximity of the intimal surface. However, these concepts consider rheological issues to be critical determinants and consider the arterial wall to be relatively passive. Another hypothesis, linking wall shear stress with atherosclerosis, emerged in the 2000s in light of various works (Gimbrone 1998; Ross *et al.* 2004) on the active participation of arterial-wall cells in pathology processes.

It is now clearly established that hemodynamic factors, in the form of mechanical stimuli of endothelial cells lining the intimal layer of the vascular wall, regulate many of the physiological responses of the healthy arterial wall and are also involved in the development of pathologies of the

arterial wall, such as atherosclerosis, intimal hyperplasia, dilatations and even ruptures. Endothelial cells are primary sensors of wall shear stress and function as sensors of mechanical loads in the wall's biological responses (Tarbell *et al.* 2014). This concept of mechanotransducing endothelium indicates that any change in mechanical stimuli of the endothelial surface – values, orientations, variations, etc. – can cause dysfunction and hence initiate the different processes of development of pathologies in the vascular wall.

In healthy humans, the instantaneous wall shear stress values can vary from 10 to 70 dyn/cm² (1–7 Pa) in the straight arteries of the vascular system (Malek *et al.* 1999). Thus, the order of magnitude of the mean physiological values commonly found in the literature for straight arteries is 15–20 dyn/cm² (Malek *et al.* 1999). These values, called reference values, are classified as atheroprotective and/or conform with the wall stresses to which vascular endothelial cells may be subjected without expressing “corrective” responses to return to the reference value.

Wall shear stress values, however, whether at reference values or above or below reference values, are subject to debate. At present, there is no sufficiently accurate *in vivo* methodology for measuring deformable-wall velocity gradients in the thickness of unsteady boundary layers. MRI measurements, for example, cannot be performed with a resolution finer than 1.5 mm. Numerical simulations, meanwhile, which enable quantification of physical quantities as near as necessary to the wall, depend on the fluid models and structures used to reproduce the vascular segment under investigation, the geometries retained to represent those segments and the boundary conditions deployed. Finally, *in vitro* measurements can present the same disadvantages as *in silico* models, and near-wall quantifications are difficult to implement.

Beyond the difficulty in establishing precise yield values above or below which deleterious processes are possible, the following sections take stock of the trends and controversies combining geometric singularities, low, high and very high values of wall shear stress and its derived indexes, their spatio-temporal variations and pathologies. The dynamics of VSs, representative of fluid transport, are also being investigated as a hemodynamic marker that can be associated with the development of vascular pathologies.

It is essential to underline that although *in vitro* and *in silico* models serve to establish and analyze hemodynamic indexes, the correlations between these markers and vascular pathologies can only be confirmed *in fine* through *in vivo* clinical studies.

3.5.1. WSS and pathologies

If we consider the wall shear stress values between 15 and 20 dyn/cm² as reference values in a healthy human, it is now commonly accepted that values below or equal to 5 dyn/cm² are low WSS values (Sho *et al.* 2004), values greater than 30 dyn/cm² are high values (Dolan *et al.* 2011) and values greater than or equal to 120 dyn/cm² are very high values that act on circulating cells (Moake *et al.* 1988). As we saw in section 3.4, the downstream of cross-section constrictions, bifurcations, curvatures and enlargements of cross-section result in near-wall separation zones occupied by low-velocity flows that can cause low wall shear stress values. In contrast, accelerated flow in the form of a jet results in velocity gradients and, as a result, high near-wall shear stress values and very high values at the cross-section constriction neck. Fluid shear rates are also high.

3.5.1.1. Low WSS values

Having demonstrated the roles played by high residence times (RRTs) of circulating particles and increased endothelial wall permeability subjected to low wall shear stress values in pathologies such as atherosclerosis, new concepts have emerged to better understand the link between hemodynamic markers and pathology. For example, the introduction of the unsteady nature of flows in the different *in vitro* and *in silico* models led to the appearance of the criterion of high oscillating WSS, that is, a high OSI index, as an additional predictive indicator of arterial remodeling (Ku *et al.* 1985). The low WSS hypothesis then evolved into a combined low WSS and high OSI hypothesis. This criterion is now widely used and has been identified as a predictor of zones promoting the development of intimal thickening, either from *in vivo* animal models (Cheng *et al.* 2006; Thim *et al.* 2012), or in experimental models (Moore *et al.* 1994; Ding *et al.* 2001) and *in silico* models (Steinman *et al.* 2002; Ene-Irodache and Remuzzi 2012), who directly correlate their measurements with clinical observations.

In parallel, DePaola *et al.* (1992), in an experimental study on endothelial cells of bovine aorta, also demonstrate the importance of spatial wall shear stress gradients, WSSG, promoting stretching (WSSG > 0) or compression

(WSSG < 0) of endothelial cells and subsequently influencing their shape, migration and division capacity. Depending on the WSSG level, the wall permeability can also be altered, as discussed by Lei *et al.* (1996), Herrmann *et al.* (1994) or Buchanan *et al.* (1999). In addition, the zones, subject to low and oscillating wall shear stress values, extend or reduce due to flow pulsatility, resulting in strong temporal WSS gradients at the cardiac cycle scale. The works of White *et al.* (2001), Haidekker *et al.* (2001), or Soulis *et al.* (2006) suggest that this temporal variation plays a role in the increase in intimal proliferation.

Thus, the theory of low and oscillating wall shear stress appears to potentially minimize a more complex reality of the links between hemodynamic markers and arterial remodeling. In line with the works of Peiffer *et al.* (2013a) and based on studies by Wang *et al.* (2013), showing that endothelial cells are sensitive to flow multidirectionality, Morbiducci *et al.* (2015) combine the complexity of the links between markers and pathology by exploring the role played by the multi-directionality of wall shear stress. Recent reviews of the literature (Barakat 2013; Peiffer *et al.* 2013b) also question both the systematic generalization of the criterion “low and oscillating wall shear stress” and its universally predictive nature. Indeed, whatever the vascular pathology, it is difficult to compare similar geometric characteristics (curvature, dilatation, constriction, etc.) presenting significant local variabilities from one arterial site to another, from one patient to another, from one study time to another, or indeed from one animal model to another.

3.5.1.2. High WSS values

In the general case of arterial dilatations – aneurysms of the thoracic or abdominal aorta, intracranial and dissection – there are two opposing theories – high and low wall shear stress values – to explain the same development of the pathology.

In *in vivo* studies based on human MRI measurements, Hope *et al.* (2011), Mahavedia *et al.* (2014) and Rodriguez-Palomares *et al.* (2018) highlight an increase in the maximum value of wall shear stress in the dilated ascending aorta downstream of a bicuspid valve relative to the values encountered in healthy cases downstream of a tricuspid valve. High WSS values are also reported in studies correlating measurements *in silico* and clinical patient monitoring for sacciform intracranial aneurysms (Castro *et al.* 2009), or indeed during the aneurysmal evolution of the false lumen of

dissections (Shang *et al.* 2015). The effects of high WSS were also explored *in vitro* on bovine aortic endothelial cells in conjunction with the application of a WSSG, showing that the addition of a positive WSSG exacerbates cell dysfunction, significantly altering their alignment and increasing cell death (Dolan *et al.* 2011).

In contrast, low wall shear stresses are observed *in vivo* in the dilated ascending aorta (Burk *et al.* 2012) and in *in silico* studies with patient-specific geometry, correlating measurements and the patients' clinical profile, in the false lumen of dissections (Karmonik *et al.* 2013; Doyle *et al.* 2014), in intracranial aneurysms (Boussel *et al.* 2008; Zhou *et al.* 2017) or abdominal aneurysms (Boyd *et al.* 2016). In the case of aneurysms, it should be noted that the morphology is generally fusiform.

This low/high wall shear stress controversy is discussed by Meng *et al.* (2014). The differentiated activation of the channels of the biological cascade in the mechanical transduction, notably with an inflammatory pathway – associated with low WSS – and an increase in metalloproteinase expression and activity – correlated with high WSS – seems to be at the origin of the differences observed. Moreover, *in vitro* studies confirm these two pathways: Anidjar *et al.* (1992) show a correlation between aortic enlargement and activation of the inflammatory system using an animal (rat) model of arterial enlargement. Sho *et al.* (2002), meanwhile, confirm, on another animal model (rabbit), an increasing activity of metalloproteinases following the exposure of the wall to strong WSS. Fedak *et al.* (2003) show, in samples of dilated ascending aorta collected from patients with a bicuspid valve, an increase in metalloproteinase activity that is correlated with aortic diameter. Finally, thanks to 4D flow MRI measurements, Guzzardi *et al.* (2015) also report that downstream of a bicuspid valve, ascending aorta dilatation is associated with high WSS values corresponding to extracellular matrix deregulation, the degeneration of elastin fibers and an increase in metalloproteinase expression.

In light of the sometimes divergent conclusions of these different studies putting forward a hypothesis of low or high WSS in the dilatation process, it will, without a doubt, be necessary to question the role of biological and biochemical mechanisms taking place at the cellular or molecular scale and intervening in mechanotransduction: a change of scale for a change of paradigm.

3.5.2. Hemodynamic markers and thrombus

The thrombus can roughly be described as a blood clot forming in various pathologies such as atherosclerosis, aneurysms of the abdominal aorta, dissections, etc. Its presence participates in an alteration of the pathological process. We will not discuss its protective or deleterious role with regard to pathologies here, but we will discuss the mechanisms of its formation that are linked to the hemodynamics. Platelets and circulating blood cells contribute to thrombus formation through their activation, aggregation and adhesion to the arterial wall; these three steps are complementary.

3.5.2.1. Thrombus and high WSS values

In accelerated flow in the form of a jet, such as at the neck of an arterial stenosis or at an aortic dissection entry tear, high near-wall velocity gradients appear and give rise to high WSS values (of the order of 125 dyn/cm^2 (Deplano and Siouffi 1999) and 100 dyn/cm^2 (Khannous *et al.* 2019), respectively) as well as very high fluid shear values (of the order of $5,000 \text{ s}^{-1}$; Casa *et al.* 2015).

This configuration draws platelets and blood proteins such as von Willebrand factor² (vWF) towards the walls. This is known as the margination phenomenon (Zhao *et al.* 2007). In the presence of thrombogenic surfaces such as subendothelial collagen fibers, exposed as a result of endothelium stripping, vWFs will rapidly colonize these surfaces. Given high fluid shear rates, (i) vWFs distort and stretch to form nets, multiplying platelet adhesion contacts and sites, and (ii) platelets will bind to these proteins rather than to fibrinogen, another coagulation factor; platelets rapidly adhere and aggregate even before their activation, as shown in vitro by Ruggeri *et al.* (2006) and in silico by Wellings *et al.* (2012). High shear rates also allow rapid platelet accumulation and activation, as observed in vitro by Bark *et al.* (2012). In addition, high WSS values also cause platelet activation (Moake *et al.* 1988). During the activation phase, platelets release proteins, notably vWF proteins and fibrinogen. In the case where platelets have already adhered, this release will allow thrombus growth. By constricting the cross-section of the arterial lumen slightly further, shear rates increase and the process self-maintains, to the extent of possibly occluding the vessel (Casa *et al.* 2015).

² von Willebrand factor is a protein that allows platelet adhesion to the arterial wall.

Thrombi that adhere in zones of high WSS are generally more unstable than those formed in zones of low WSS, given the bonds involved for platelet aggregation (Shi *et al.* 2016). The instability of thrombi formed in this way may lead to partial or total detachment of the thrombus, which gives rise to risks of the occlusion of a downstream artery with a smaller diameter.

3.5.2.2. *Thrombus and low WSS values*

Low WSS values found in zones of recirculation, for example, aneurysm, or other zones presenting cross-section enlargement, appear to favor adhesion of platelets preferentially via the fibrinogen present, as shown in vitro by Savage *et al.* (1996), in a study conducted on blood from human donors. Back in the 1970s, Blackshear *et al.* (1971), as well as Karino and Goldsmith (1977), demonstrated that the recirculation regions, the site of low WSS values, were favorable for thrombus formation. Other, more recent, studies have also correlated the presence of low wall TAWSS with the presence of thrombus, notably in the false lumen of aortic dissection. Zones of flow recirculating at low velocities (Chen *et al.* 2013; Cheng *et al.* 2015) or even of stagnant flow (Rinaudo and Pasta 2014), essentially dominated, as we have seen, by low TAWSSs and RRTs of fairly high circulating particles (Cheng *et al.* 2013; Cheng *et al.* 2015), therefore represent regions favorable to thrombus development (Meng *et al.* 2014; Menichini and Xu 2016).

It should be noted that, again, differences may appear here, underlining the complexity of the process: the in silico study by Di Achille *et al.* (2014) correlates, with clinical observations, low WSS and high OSI values with zones of the aneurysm sac of the abdominal aorta presenting thrombus in the patients under consideration. O'Rourke *et al.* (2012), meanwhile, also suggest, through in silico measurements, a combination of low WSS and low OSI values to correlate with thrombus growth zones based on two-stroke clinical imaging for patient follow-up.

3.5.2.3. *Thrombus and coherent structures*

In parallel to the concept of shear yield values within the fluid and/or at the wall as a platelet-stress mechanism acting on thrombus formation, several research groups have taken an interest in the role played by VSs, whether concerning aneurysms or aortic dissections (TAD) (Basciano *et al.* 2011; Biasetti *et al.* 2011; Ab Naim *et al.* 2016; Menichini *et al.* 2018). Through in silico models and using the criterion λ_2 to identify VSs, the

retained mechanisms clearly presented by Biasetti *et al.* (2011) in the case of abdominal aortic aneurysms (AAA) can be summarized in four phases: (i) platelets are trapped in VSs formed at the proximal throat of an aneurysm or at the entry tear of the false lumen of a TAD. (ii) The platelets, trapped in the VSs, are activated by the high shear values existing at the periphery of VSs and/or by the high WSS values that exist at the TAD entry tears. (iii) The VSs transport and convect the activated platelets downstream. (iv) In the deceleration phase, the VSs impact at the distal wall or dislocate near-wall, releasing activated platelets that aggregate and/or adhere to the wall in zones of low WSS.

The multiphysics model for modeling thrombus formation and growth, proposed by Biasetti *et al.* (2012), confirms the concept of activation/convection/release/aggregation of platelet elements.

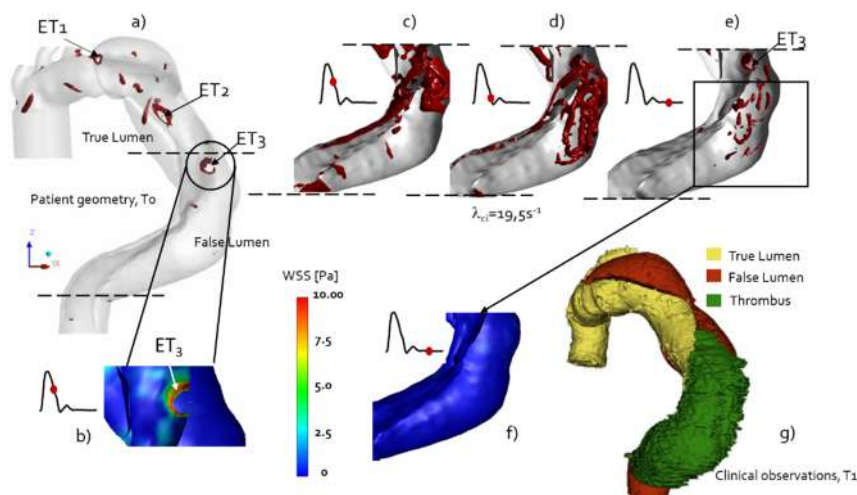


Figure 3.7. a) Geometry of a patient with type-A aortic dissection treated at T_0 by a prosthesis on the ascending-aorta segment and having residual type-B dissection. Three entry tears (ET_i) are present. b) WSS at the neck of ET_3 presenting values $>100 \text{ dyn/cm}^2$. c–e) Evolution of coherent structures in the false lumen. f) Low WSS values in coherent structure dislocation zones. g) Clinical findings 1 year after T_0 , showing thrombus formation in the false lumen. Adapted from Khannous *et al.* (2019). For a color version of this figure, see www.iste.co.uk/deplano/biological.zip

The works carried out by Khannous *et al.* (2019) within a residual type-B aortic dissection model enable this concept to be illustrated (Figure 3.7). In this unsteady 3D *in silico* model of a fluid with shear-thinning behavior, the criterion λ_{ci} is used as an identifier of coherent structures in a geometry of a patient at T_0 , presenting an unfavorable evolution one year later (T_1). Analysis performed at T_0 of the evolution of coherent structures in the false lumen and the spatiotemporal mapping of WSS shows that all of the ingredients are combined to initiate thrombus formation in the false lumen of the dissection. This result is confirmed by clinical observations made one year later at T_1 .

3.6. Conclusion and perspectives

In vitro and/or *in silico* models are implementing increasingly complex multi-physical models to closely approximate the pathophysiological reality of vascular pathologies. Thanks to advances in medical imaging, the focus in recent years is on *in vivo* validation and even inter-validation. Indeed, *in vivo* measurements validate *in vitro* and/or *in silico* modeling, but the accuracy of *in vivo* assessments of hemodynamic markers based on 4D flow MRI acquisitions, for example, must be validated by *in vitro* and/or *in silico* models. Thus, these non-invasive *in vivo* assessments at the patient's bed are of particular relevance as a diagnostic aid or in patient follow-up.

However, the understanding of the mechanisms for the initiation and development of vascular pathologies needs to be further improved. This is demonstrated by the controversies discussed in this chapter on the links between hemodynamic markers and pathologies. As such, multi-scale, growth and remodeling aspects must be included long term in the models developed. The recent technological advances in observations and measurements at the microscopic scale are enabling an ever greater understanding of the multi-scale aspect, and consequently, models are better equipped to take into account mechanisms at the cellular or indeed molecular scale. The mechanical-biological and biochemical mechanisms of arterial wall growth and remodeling are complex and their modeling remains only partial. Without being trite, the new possibilities linked to deep learning and processing by large databases will no doubt enable analysis of the correlations made between pathologies and hemodynamic indexes (or any other markers) on a large number of patients, and deduce associations that are useful to patient care.

3.7. References

- Ab Naim, W.N., Ganesan, P.B., Sun, Z., Liew, Y.M., Qian, Y., Lee, C.J., Jansen, S., Hashim, S.A., Lim, E. (2016). Prediction of thrombus formation using vortical structures presentation in Stanford type B aortic dissection: A preliminary study using CFD approach. *Appl. Math. Model.*, 40(4), 3115–3127.
- Alimohammadi, M., Pichardo-Almarza, C., Agu, O., Diaz-Zuccarini, V. (2016). Development of a patient-specific multi-scale model to understand atherosclerosis and calcification locations: Comparison with in vivo data in an aortic dissection. *Front. Physiol.*, 7, 238.
- Anidjar, S., Dobrin, P.B., Eichorst, M., Graham G.P., Chejfec, G. (1992). Correlation of inflammatory infiltrate with the enlargement of experimental aortic aneurysms. *J. Vasc. Surg.*, 16(2), 139–147.
- Arzani, A. and Shadden, S.C. (2012a). Flow topology in patient-specific abdominal aortic aneurysms during rest and exercise. *APS Division of Fluid Dynamics Meeting Abstracts, APS Meeting Abstracts*, G16.001.
- Arzani, A. and Shadden, S.C. (2012b). Characteristics of the transport topology in patient-specific abdominal aortic aneurysm models. *Phys. Fluids*, 24, 081901.
- Barakat, A.I. (2013). Blood flow and arterial endothelial dysfunction: Mechanisms and implications. *C.R. Physiques*, 14, 479–496.
- Bark, D.L., Para, A.N., Ku, D.N. (2012). Correlation of thrombosis growth rate to pathological wall shear rate during platelet accumulation. *Biotechnol. Bioeng.*, 109, 2642–2650.
- Barker, A.J., Lanning, C., Shandas, R. (2010). Quantification of hemodynamic wall shear stress in patients with bicuspid aortic valve using phase-contrast MRI. *Ann. Biomed. Eng.*, 38(3), 788–800.
- Basciano, C., Kleinstreuer, C., Hyun, S., Finol, E.A. (2011). A relation between near-wall particle-hemodynamics and onset of thrombus formation in abdominal aortic aneurysms. *Ann. Biomed. Eng.*, 39(7), 2010–2026.
- Biasetti, J., Hussain, F., Gasser, T.C. (2011). Blood flow and coherent vortices in the normal and aneurysmatic aortas: A fluid dynamical approach to intraluminal thrombus formation. *J. R. Soc. Interface*, 8, 1449–1461.
- Blackshear, P.L., Forstrom, R.J., Lorberbaum, M., Gott, V.L., Sovilj, R. (1971). A role of flow separation and recirculation in thrombi formation on prosthetic surfaces. *AIAA 9th Aerospace Meeting Paper*, 71–103.

- Boiron, O., Deplano, V., Pelissier, R. (2007). Experimental and numerical studies on the starting effect on the secondary flow in a bend. *J. Fluid Mech.*, 574, 109–129.
- Boussel, B., Rayz, V., McCulloch, C., Martin, A., Acevedo-Bolton, G., Lawton, M., Higashida, R., Smith, W.S., Young, W.L., Saloner, D. (2008). Aneurysm growth occurs at region of low wall shear stress. *Interface*, 39, 2997–3002.
- Boyd, A.J., Kuhn, D.C.S., Lozowy, R.J., Kulbisky, G.P. (2016). Low wall shear stress predominates at sites of abdominal aortic aneurysm rupture. *J. Vasc. Surg.*, 63(6), 1613–1619.
- Buchanan J.R., Kleinstreuer C., Truskey G., Lei M. (1999). Relation between non-uniform hemodynamics and sites of altered permeability and lesion growth at the rabbit aorto-celiac junction. *Atherosclerosis*, 143, 27–40.
- Bürk, J., Blanke, P., Stankovic, Z., Barker, A., Russe, M., Geiger, J., Frydrychowicz, A., Langer, M., Markl, M. (2012). Evaluation of 3D blood flow patterns and wall shear stress in the normal and dilated thoracic aorta using flow-sensitive 4D CMR. *J. Cardiovasc. Magn. Reson.*, 14, 84.
- Caro, C.G., Fitz-Gerald, J.M., Schroter, R.C. (1971). Atheroma and arterial wall shear – Observation, correlation and proposal of a shear dependent mass transfer mechanism for atherogenesis. *Proc. Roy. Soc. Land. B*, 177, 109–133.
- Casa, L.D.C., Deaton, D.H., Ku, K.N. (2005). Role of high shear rate in thrombosis. *J. Vasc. Surg.*, 61(4), 1068–1080.
- Castro, M.A., Putman, C.M., Sheridan, M.J., Cebal, J.R. (2009). Hemodynamic patterns of anterior communicating artery aneurysms: A possible association with rupture. *Am. J. Neuroradiol.*, 30(2), 297–302.
- Chakraborty, P., Balachandar, S., Adrian, R.J. (2005). On the relationships between local vortex identification schemes. *J. Fluid Mech.*, 535, 189214.
- Chen, D., Müller-Eschner, M., Kotelis, D., Böckler, D., Ventikos, Y., von Tengg-Kobligk, H. (2013). A longitudinal study of type-B aortic dissection and endovascular repair scenarios: Computational analysis. *Med. Eng. Phys.*, 35, 320–330.
- Cheng, K.C. and Mok, S.Y. (1986). Flow visualization studies on secondary flow patterns and centrifugal instability phenomena in curved tubes. *Fluid Control and Measurement*, 2, 765–773.
- Cheng, C., Tempel, D., Haperen, R., Baan, A., Grosveld, F., Daemen, M., Krams, R., Crom, R. (2006). Atherosclerotic lesion size and vulnerability are determined by patterns of fluid shear stress. *Circ.*, 113, 2744–2753.

- Cheng, Z., Riga, C., Chan, J., Hamady, M., Wood, N.B., Cheshire, N.J., Xu, Y., Gibbs, R.G.J. (2013). Initial findings and potential applicability of computational simulation of the aorta in acute type B dissection. *J. Vasc. Surg.*, 57, 35–43.
- Cheng, Z., Wood, N.B., Gibbs, R.G., Xu, X.Y. (2015). Geometric and flow features of type B aortic dissection: Initial findings and comparison of medically treated and stented cases. *Ann. Biomed. Eng.*, 43(1), 177–189.
- Chong, M.S., Perry, A.E., Cantwel, B.J. (1990). A general classification of three-dimensional flow fields. *Phys. Fluid. A*, 2, 765–777.
- Dasi, L.P., Simon, H.A., Sucusky, P., Yoganathan, A.P. (2009). Fluid mechanics of artificial heart valves. *Clin. Exp. Pharmacol. P.*, 36, 225–237.
- Dean, W.R. (1928). The streamline motion of fluid in a curved pipe. *Phil. Mag.*, 7, 673–695.
- Dennis, S.C.R. and Ng, M. (1982). Dual solutions for steady laminar flow through a curved tube. *Quart. J. Mech. Appl. Math.*, 35, 305–324.
- DePaola, N., Gimbrone M.A., Davies, P.F., Dewey C.F. (1992). Vascular endothelium responds to fluid shear stress gradients. *Arterioscler. Thromb.*, 12, 1254–1257.
- Deplano, V. and Siouffi, M. (1999). Experimental and numerical study of pulsatile flows through stenosis: Wall shear stress analysis. *J. Biomech.*, 32, 1081–1090.
- Deplano, V., Knapp, Y., Bertrand, E., Gaillard, E. (2007). Flow behaviour in an asymmetric compliant experimental model for abdominal aortic aneurysm. *J. Biomech.*, 40(11), 2406–2413.
- Deplano, V., Knapp, Y., Bailly, L., Bertrand, E., (2014). Flow of a blood analogue fluid in a compliant abdominal aortic aneurysm model: Experimental modelling. *J. Biomech.*, 47(6), 1262–1269.
- Deplano, V., Guivier-Curien, C., Bertrand, E. (2016). 3D analysis of vortical structures in an abdominal aortic aneurysm by stereoscopic PIV. *Exp. Fluids*, 57, 167.
- Di Achille P., Tellides, G., Figueroa, C.A., Humphrey J.D. (2014). A haemodynamic predictor of intraluminal thrombus formation in abdominal aortic aneurysms. *Proc. R. Soc. A.*, 470, 20140163.
- Ding, Z., Wang, K., Li, J., Cong, X. (2001). Flow field and oscillatory shear stress in a tuning-fork-shaped model of the average human carotid bifurcation. *J. Biomech.*, 34(12), 1555–1562.

- Dolan, J.M., Meng, H., Singh, S., Paluch, R., Kolega, J. (2011). High fluid shear stress and spatial shear stress gradients affect endothelial proliferation, survival, and alignment. *Ann. Biomed. Eng.*, 39, 1620–1631.
- Doyle, B.J. and Norman, P.E. (2016). Computational biomechanics in thoracic aortic dissection: Today's approaches and tomorrow's opportunities. *Ann. Biomed. Eng.*, 44, 71–83.
- Ene-Iordache, B. and Remuzzi, A. (2012). Disturbed flow in radial-cephalic arteriovenous fistulae for haemodialysis: Low and oscillating shear stress locates the sites of stenosis. *Nephrol. Dial. Transpl.*, 27(1), 358–368.
- Fedak, P.W.M., De Sa, M.P.L., Verma, S., Nili, N., Kazemian, P., Butany, J., Strauss, B.H., Weisel, R.D., David, T.E. (2003). Vascular matrix remodeling in patients with bicuspid aortic valve malformations: Implications for aortic dilatation. *J. Thorac. Cardiovasc. Surg.*, 126(3), 797–805.
- Fry, D.L. (1968). Acute vascular endothelial changes associated with increased blood velocity gradients. *Circ. Research*, 22, 165–197.
- Fung, Y.C. (1996). *Biomechanics: Circulation*, 2nd edition. Springer-Verlag, New York.
- Gimbrone Jr., M.A. and Topper, J.N. (1998). Biology of the vessel wall: Endothelium. In *Molecular Basis of Heart Diseases*, Chien, K.R. (ed). Harcourt Brace, Troy, MO.
- Grigioni, M., Daniele, C., Morbiducci, U., Del Gaudio, C., D'Avenio, G., Balducci, A., Barbaro, V. (2005). A mathematical description of blood spiral flow in vessels: Application to a numerical study of flow in arterial bending. *J. Biomech.*, 38(7), 1375–1386.
- Guivier, C., Deplano, V., Bertrand, E. (2009). Validation of a numerical 3-D fluid–structure interaction model for a prosthetic valve based on experimental PIV measurements. *Med. Eng. Phys.*, 31, 986–993.
- Guzzardi, D.G., Barker, A.J., van Ooij, P., Malaisrie, S.C., Puthumana, J.J., Belke, D.D., Mewhort, H.E.M., Svystonyuk, D.A., Kang, S., Verma, S., Collins, J., Carr, J., Bonow, R.O., Markl, M., Thomas, J.D., McCarthy, P.M., Fedak, P.W.M. (2015). Valve-related hemodynamics mediate human bicuspid aortopathy. *J. Am. Coll. Cardiol.*, 66(8), 892–900.
- Haidekker, M.A., White, C.R., Frangos, J.A. (2001). Analysis of temporal shear stress gradients during the onset phase of flow over a backward-facing step. *J. Biomech Eng.*, 123, 455–463.

- Haller, G. (2015). Lagrangian coherent structures. *Annu. Rev. Fluid Mech.*, 47(1), 137–162.
- Hasenkam, J.M., Giersiepen, M., Reul, H., (1988). Three-dimensional visualization of velocity fields downstream of six mechanical aortic valves in a pulsatile flow model. *J. Biomech.*, 21, 647–661.
- Hermann, R.A., Malinauskas, R.A., Truskey, G.A. (1994). Characterization of sites with elevated LDL permeability at intercostal, celiac, and iliac branches of the normal rabbit aorta. *Arterioscler. Thromb.*, 14, 313–323.
- Himburg, H.A., Grybowski, D.M., Hazel, A.L., LaMarck, J.A., Li, X.M., Friedman, M.H. (2004). Spatial comparison between wall shear stress measures and porcine arterial endothelial permeability. *Am. J. Phys. – Heart Circ. Phys.*, 286, 1916–1922.
- Hope, M.D., Hope, T.A., Crook, S.E., Ordovas, K.G., Urbania, T.H., Alley, M.T., Higgins, C.B. (2011). 4D flow CMR in assessment of valve-related ascending aortic disease. *JACC Cardiovasc. Imaging*, 4, 781–787.
- Hunt, J.C.R., Wray, A.A., Moin, P. (1988). Eddies, stream, and convergence zones in turbulent flows. *Center for Turbulence Research Report*. CTR-S88, 193–208.
- Jeong, J., Hussain, F., Schoppa, W., Kim, J. (1997). Coherent structures near the wall in a turbulent channel flow. *J. Fluid Mech.*, 332, 185–214.
- Joly, F., Soulez, G., Garcia, D., Lessard, S., Kauffmann, C. (2018). Flow stagnation volume and abdominal aortic aneurysm growth: Insights from patient-specific computational flow dynamics of Lagrangian-coherent structures. *Comput. Biol. Med.*, 92, 98–109.
- Karino, T. and Goldsmith, H.L. (1977). Flow behaviour of blood cells and rigid spheres in an annular vortex. *Phil. Trans. R. Soc. Lond. B*. 279, 413–445.
- Karmonik, C., Müller-Eschner, M., Partovi, S., Geisbüsch, P., Ganten, M.-K., Bismuth, J., Davies, M.G., Böckler, D., Loebe, M., Lumsden, A.B., von Tengg-Kobligk, H. (2013). Computational fluid dynamics investigation of chronic aortic dissection hemodynamics versus normal aorta. *Vasc. Endovasc. Surg.*, 47(8), 625–631.
- Khannous, F., Gaudry, M., Guivier-Curien, C., Piquet, P., Deplano, V. (2019). How can flow dynamics predict clinical evolution of residual type B aortic dissection? *Comput. Meth. Biomech. Biomed. Eng.*, 22(1), S99–S101.
- Kilner, P.J., Yang, G.Z., Mohiaddin, R.H., Firmin, D.N., Longmore, D.B. (1993). Helical and retrograde secondary flow patterns in the aortic arch studied by three-directional magnetic resonance velocity mapping. *Circ.*, 88, 2235–2247.

- Kim, G.B., Hojin, H., Kweon, J., Lee, S.J., Kim Y., Yang, D.H., Kim, N. (2016). Post-stenotic plug-like jet with a vortex ring demonstrated by 4D flow MRI. *Magn. Reson. Imaging*, 34, 371–375.
- Ku, D.N., Giddens, D.P., Zarins, C.K., Glagov, S. (1985). Pulsatile flow and atherosclerosis in the human carotid bifurcation. Positive correlation between plaque location and low oscillating shear stress. *Arteriosclerosis*, 5, 293–302.
- Lei, M., Kleinstreuer, C., Truskey, G.A. (1996). A focal stress gradient-dependent mass transfer mechanism for atherogenesis in branching arteries. *Med. Eng. Phys.*, 18(4), 326–332.
- Lyne, W.H. (1971). Unsteady viscous flow in a curved pipe. *J. Fluid Mech.*, 45, 13.
- Mahadvia, R., Barker, A.J., Schnell, S., Entezari, P., Kansal, P., Fedak, P.W.M., Malaisrie, C., McCarthy, P., Collins, J., Carr, J., Marki, M. (2014). Bicuspid aortic cusp fusion morphology alters aortic three-dimensional outflow patterns, wall shear stress, and expression of aortopathy. *Circ.*, 129(6), 673–682.
- Malek, A.M., Alper, S.L., Izumo, S. (1999). Hemodynamic shear stress and its role in atherosclerosis. *JAMA*, 282(21), 2035–2042.
- Masliyah, J.H. (1980). On laminar flow in curved semicircular ducts. *J. Fluids Mech.*, 99(3), 469–479.
- McDonald, D.A. (1952). The velocity of blood flow in the rabbit aorta studied with high-speed cinematography. *J. Physiol.*, 118, 328–339.
- Meierhofer, C., Schneider, E.P., Lyko, C., Hutter, A., Martinoff, S., Markl, M., Hager, A., Hess, J., Stern, H., Fratz, S. (2013). Wall shear stress and flow patterns in the ascending aorta in patients with bicuspid aortic valves differ significantly from tricuspid aortic valves: A prospective study. *Eur. Heart J. – Cardiovasc. Imag.*, 14(8), 797–804.
- Meng, H., Tutino, V.M., Xiang, J., Siddiqui, A. (2014). High WSS or low WSS? Complex interactions of hemodynamics with intracranial aneurysm initiation, growth, and rupture: Toward a unifying hypothesis. *Am. J. Neuroradiol.*, 35(7), 1254–1262.
- Menichini, C. and Xu, X.Y. (2016). Mathematical modeling of thrombus formation in idealized models of aortic dissection: Initial findings and potential applications. *J. Math. Biol.*, 73, 1205–1226.
- Menichini, C., Cheng, Z., Gibbs, R.G.J., Xu, X.Y. (2016). Predicting false lumen thrombosis in patient-specific models of aortic dissection. *J. R. Soc. Interface*, 13, 20160759.

- Moake, J.L., Turner, N.A., Statopoulos, N.A., Nolasco, L., Hellums, J.D. (1988). Shear-induced platelet aggregation can be mediated by vWF released from platelets, as well as by exogenous large or unusually large vWF multimers, requires adenosine diphosphate and is resistant to aspirin. *Blood*, 71(5), 1366–1374.
- Moore, J.E., Xu, C., Glagovb, S., Zarinsc, C.K., Ku, D.N. (1994). Fluid wall shear stress measurements in a model of the human abdominal aorta: Oscillatory behavior and relationship to atherosclerosis. *Atherosclerosis*, 10(2), 225–240.
- Morbiducci, U., Ponzini, R., Rizzo, G., Cadioli, M., Esposito, A., De Cobelli, F., Del Maschio, A., Montecvecchi, F.M., Redaelli, A. (2009). In vivo quantification of helical blood flow in human aorta by time-resolved three-dimensional cine phase contrast magnetic resonance imaging. *Ann. Biomed. Eng.*, 37(3), 516–531.
- Morbiducci, U., Ponzini, R., Rizzo, G., Cadioli, M., Esposito, A., Montecvecchi, F.M., Redaelli, A. (2011). Mechanistic insight into the physiological relevance of helical blood flow in the human aorta: An in vivo study. *Biomech. Model. Mechanobiol.*, 10, 339–355.
- Morbiducci, U., Gallo, D., Cristofanelli, S., Ponzini, R., Deriu, M.A., Rizzo, G., Steinman, D.A. (2015). A rational approach to defining principal axes of multidirectional wall shear stress in realistic vascular geometries, with application to the study of the influence of helical flow on wall shear stress directionality in aorta. *J. Biomech.*, 48(6), 899–906.
- Novaro, G.M., Mishra, M., Griffin, B.P. (2003). Incidence and echocardiographic features of congenital unicuspid aortic valve in an adult population. *J. Heart Valve Dis.*, 12, 674–678.
- Oh, J.K., Seward, J.B., Tajik, A.J. (1999). Valvular heart disease. In *The Echo Manual*, 2nd edition. Lippincott Williams & Wilkins, Philadelphia.
- O'Rourke, M.J., McCullough, J.P., Kelly, S. (2012). An investigation of the relationship between hemodynamics and thrombus deposition within patient-specific models of abdominal aortic aneurysm. *Proceedings of the Institution of Mechanical Engineers, Part H: J. Eng. Med.*, 226(7), 548–564.
- Pedley, T. (1980). *The Fluid Mechanics of Large Blood Vessels*. Cambridge University Press, Cambridge.
- Peiffer, V., Sherwin, S.J., Weinberg, P.D. (2013a). Computation in the rabbit aorta of a new metric – the transverse wall shear stress – to quantify the multidirectional character of disturbed blood flow. *J. Biomech.*, 46(15), 2651–2658.

- Peiffer, V., Sherwin, S.J., Weinberg, P.D. (2013b). Does low and oscillatory wall shear stress correlate spatially with early atherosclerosis? A systematic review. *Cardiovasc. Res.*, 99(2), 242–250.
- Rinaudo, A. and Pasta, S. (2014). Regional variation of wall shear stress in ascending thoracic aortic aneurysms. *Proceedings of the Institution of Mechanical Engineers, Part H: J. Eng. Med.*, 228(6), 627–638.
- Rodríguez-Palomares, J.F., Dux-Santoy, L., Guala, A., Kale, R., Maldonado, G., Teixidó-Turà, G., Galian, L., Huguet, M., Valente, F., Gutiérrez, L., González-Alujas, T., Johnson, K.M., Wieben, O., García-Dorado, D., Evangelista, A. (2018). Aortic flow patterns and wall shear stress maps by 4D-flow cardiovascular magnetic resonance in the assessment of aortic dilatation in bicuspid aortic valve disease. *J. Cardiovasc. Magn. R.*, 20, 28.
- Ross, K.A., Pyrak-Nolte, L.J., Campanella, O.H. (2004). The use of ultrasound and shear oscillatory tests to characterize the effect of mixing time on the rheological properties of dough. *Food Res. Int.*, 37(6), 567–577.
- Ruggeri, Z.M., Orje, J.N., Habermann, R., Federici, A.B., Reininger, A.J. (2006). Activation-independent platelet adhesion and aggregation under elevated shear stress. *Blood*, 108(6), 1903–1910.
- Savage, B., Saldívar, E., Ruggeri, Z.M. (1996). Initiation of platelet adhesion by arrest onto fibrinogen or translocation on Von Willebrand factor. *Cell*, 84(2), 289–297.
- Shadden, S.C. and Taylor, C.A. (2008). Characterization of coherent structures in the cardiovascular system. *Ann Biomed Eng.*, 36(7), 1152–1162.
- Shang, E.K., Nathan, D.P., Fairman, R.M., Bavaria, J.E., Gorman, R.C., Gorman, J.H., Jackson, B.M. (2015). Use of computational fluid dynamics studies in predicting aneurysmal degeneration of acute type B aortic dissections. *J. Vasc. Surg.*, 62(2), 279–284.
- Shi, X., Yang, J., Huang, J., Long, Z., Ruan, Z., Xiao, B., Xi, X. (2016). Effects of different shear rates on the attachment and detachment of platelet thrombi. *Mol. Med. Rep.*, 13, 2447–2456.
- Shimogonya, Y., Ishikawa, T., Imai, Y., Matsuki, N., Yamaguchi, T. (2009). Can temporal fluctuation in spatial wall shear stress gradient initiate a cerebral aneurysm? A proposed novel hemodynamic index, the gradient oscillatory number (GON). *J. Biomech.*, 42(11), 550–554.
- Sho, E., Sho M., Singh, T.M., Nanjo, H., Komatsu, M., Xu, C., Masuda, H., Zarins, C.K. (2002). Arterial enlargement in response to high flow requires early expression of matrix metalloproteinases to degrade extracellular matrix. *Exp. Mol. Pathol.*, 73(2), 142–153.

- Siouffi, M. (1988). Analyse des effets instationnaires sur les caractéristiques de l'écoulement en aval d'un rétrécissement local de section. PhD Thesis, University of Aix-Marseille II.
- Siouffi, M., Deplano, V., Pélissier, R. (1998). Experimental analysis of unsteady flows through a stenosis. *J. Biomech.*, 31, 11–19.
- Soulis, J.V., Giannoglou, G.D., Chatzizisis, Y.S., Farmakis, T.M., Giannakoulas, G.A., Parcharidis, G.E., Louridas, G.E. (2006). Spatial and phasic oscillation of non-Newtonian wall shear stress in human left coronary artery bifurcation: An insight to atherogenesis. *Coronary Artery Dis.*, 17(4), 351–358.
- Steinman, D.A., Thomas, J.B., Ladak, H.M., Milner, J.S., Rutt, B.K., Spence, J.D. (2002). Reconstruction of carotid bifurcation hemodynamics and wall thickness using computational fluid dynamics and MRI. *Magn. Reson. Med.*, 47, 149–159.
- Sudo, K., Sumida, M., Yamane, R. (1992). Secondary motion of fully developed oscillatory flow in a curved pipe. *J. Fluid Mech.*, 237, 189–208.
- Tadros, T.M., Klein, M.D., Shapira, O.M. (2009). Ascending aortic dilatation associated with bicuspid aortic valve. *Circ.*, 119(6), 880–890.
- Tarbell, J.M., Shi, Z.D., Dunn, J., Jo, H. (2014). Fluid mechanics, arterial disease, and gene expression. *Ann. Rev. Fluid Mech.*, 46(1), 591–614.
- Thim, T., Hagensen, M.K., Hørlyck, A., Kim, W.Y., Niemann, A.K., Thrysoe, S.A., Drouet, L., Paaske, W.P., Bøtker, H.E., Falk, E. (2012). Wall shear stress and local plaque development in stenosed carotid arteries of hypercholesterolemic minipigs. *J. Cardiovasc. Dis. Res.*, 3(2), 76–83.
- Wang, C., Baker, B.M., Chen, C.S., Schwartz, M.A. (2013). Endothelial cell sensing of flow direction. *Arterioscler. Thromb. Vasc. Biol.*, 33, 2130–2136.
- Wellings, P.J. and Ku, D.N. (2012). Mechanisms of platelet capture under very high shear. *Cardiovasc. Eng. Tech.*, 3, 161–170.
- White, C.R., Haidekker, M., Bao X., Frangos, J.A. (2001). Temporal gradients in shear, but not spatial gradients stimulate endothelial cell proliferation. *Circ.*, 103, 2508–2513.
- Yoganathan, A.P., Woo, Y.R., Sung, H.W. (1986). Turbulent shear stress measurements in the vicinity of aortic heart valve prostheses. *J. Biomech.*, 19, 433–442.
- Zhao, R., Kameneva, M.V., Antaki, J.F. (2007). Investigation of platelet margination phenomena at elevated shear stress. *Biorheology*, 44, 161–177.

- Zhou, J., Adrian, R.J., Balachandar, S., Kendall, T.M. (1999). Mechanisms for generating coherent packets of hairpin vortices in channel flow. *J. Fluid Mech.*, 387, 353–396.
- Zhou, G., Zhu, Y., Yin, Y., Su, M., Li, M. (2017). Association of wall shear stress with intracranial aneurysm rupture: Systematic review and meta-analysis. *Sci. Rep.*, 7, 5331.
- Zhu, C., Seo, J.H., Mitta, R. (2018). Computational modelling and analysis of haemodynamics in a simple model of aortic stenosis. *J. Fluid Mech.*, 851, 23–49.